7

Sol-gel dip-coated $SiO_2/(ZnO/Sn\text{-}In_2O_3)_{n=4}$/SS Semi-metallic/Dielectric multilayer based SSACs on SS tubes

7.1 Introduction

So far, various SSAC structures are reported, which are (i) semiconductor-based tandem structure, (ii) a metal-dielectric composite structure, (iii) a multilayer SSAC structure composed of alternative metal, and (iv) dielectric layers, an intrinsic absorber, a black paint, and a textured surface structure [Kennedy et al., 2002, Cao et al., 2014]. Among these, the dielectric and metal-based SSACs are the most common SSAC structures. Several cermet-based structures have been reported as SSAC for thermal applications. The metal and dielectric structure offer flexibility in the selection of the metal and dielectric compounds when a new SSAC with the desired optical properties is required to develop [Andersson et al., 1980]. Also, by varying the fraction of metal and dielectric compound, the optical properties can be tailored for optimized SSAC structure [Niklasson et al.,1981]. However, these structures experienced corrosion degradation in open environmental conditions due to the presence of metal and its tendency to react with oxygen forming metal oxides and thus, degrading the optical properties. Therefore, it is necessary to develop coating structures that can be stable in an open environment. Also, very few cermet-based structures are commercially available, and these SSAC structures are manufactured using physical vapor deposition techniques, which are vacuum-based. These vacuum-based methodologies make the deposition system complex, and the cost of production may be relatively higher. Also, for large scale coating on the receiver tubes, further, the complexity of the deposition system increases.

Further, most of the reported SSAC structures are stable only in the medium temperature range, and very few are stable at higher temperatures in vacuum only [Selvakumar & Barshilia, 2012]. Therefore, it is necessary to develop chemically and thermally stable SSACs, without degrading their optical performance at higher operating temperatures in an open environment [Kennedy & Price, 2005]. In contrast, the multilayer coating structure may be more promising to achieve greater solar absorption due to absorption induced by multiple interfaces, even for lower layer thicknesses. The smaller thickness can also help in minimizing heat loss. The multilayer absorber is composed of different metals such as molybdenum, silver, copper, nickel, and dielectrics such as aluminum oxide, silicon oxide, cerium oxide, zinc sulfide [Kennedy et al., 2002]. These structures are again subjected to the oxidation or interdiffusion of metal in oxide dielectrics.

In contrast, all oxide-based SSACs can prevent the oxidation of the metal content along with better corrosion and high-temperature stability. Given the advantages for all oxide SSACs, we have designed and developed a multilayer structure composed of transparent conductive oxide (TCO), which serves the purpose of a metallic layer and a dielectric oxide on the SS substrate using sol-gel based dip coating. The most common tin-doped indium oxide film ($Sn\text{-}In_2O_3$) is chosen as a substitute for the metal layer [Stadler, 2012], together with ZnO as the dielectric layer. These materials have a low processing temperature, as well as high optical transparency in the visible range [Janotti & Van De Walle, 2009]. These oxide layers have been synthesized using different methods of physical and chemical deposition [Kumar & Sudarshan, 1995, Liu & Zeng, 2013]. Sol-gel immersion coating is relatively easier compared to other deposition techniques. This process is environmentally friendly, less cumbersome and offers simple handling of the materials that will be used for the synthesis of thin layers. Immersion coated structures show good adhesion to a variety of substrates such as metal, glass and

ceramics. In addition, this process can be easily scaled to produce large-scale coatings, which makes it interesting to study spectrally selective coatings using the desired solution precursors [Subasri et al., 2016].

In this chapter, we are reporting the deposition and optimization of oxide-based structures for mid-range (up to 300°C) solar thermal application using sol-gel dip-coating technique. The microstructural and optical properties are discussed in detail in the result and discussion section. Also, the optimized structure is subjected to thermal and corrosion treatment to study the thermal and corrosion behavior and their impact on the optical performance of the developed SSAC structures.

7.2 Experimental details

SiO_2/ $(ZnO/Sn\text{-}In_2O_3)_{n=4}$/SS metallic/dielectric multilayers are fabricated using sol-gel dip coating. The deposition details are given in section **3.2.4.** For the deposition, an indigenously developed dip coating system at IIT Jodhpur is used. Its features are described in **Annexure A**. **Figure 7.1** shows the schematic of film coating processes using sol-gel dip coating. Here, the solution adheres while dipping the substrate inside the solution, forming a thin film during withdrawal, which can be cured at normal or high temperature if required. After drying, the process can be repeated several times to achieve the desired optical properties.

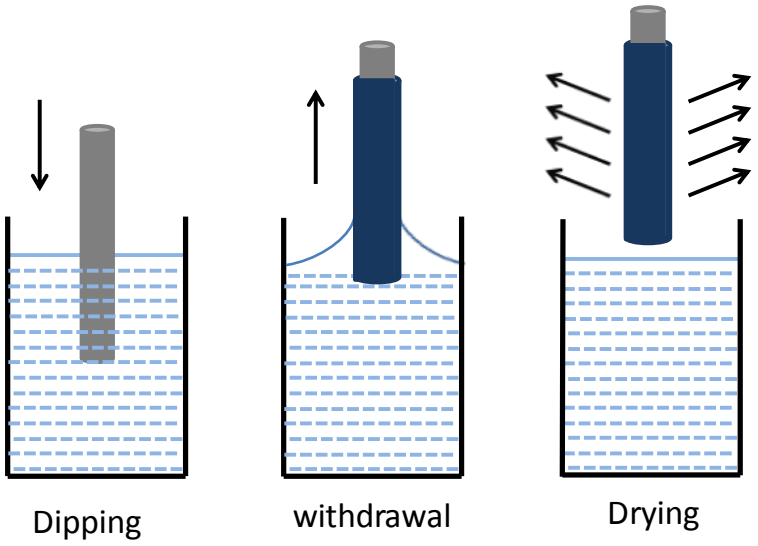

Figure 7.1 Schematic image of dip coating process for thin film fabrication

7.3 Optimization

Initially, the process was carried out on planer SS substrates. The optimization of the deposited film was investigated by increasing the number of deposited layers and simultaneously measuring their optical properties. The absorptance and emittance of the fabricated film were estimated using reflectance measurement in the UV-Vis and IR region, even with the variation of number of ZnO as dielectric and Sn- In_2O_3 as a metallic thin layers. We deposited up to six pairs of ZnO/ Sn-In_2O_3 layers and compared the estimated absorptance and emittance. **Table 7.1** summarizes the optical properties of different samples deposited during optimization. The measured reflectance plots for different layered structures are shown in **Figure 7.2**. We got optimized optical properties i.e. the maximum absorptance and minimum emittance in the desired wavelength range for four pairs of ZnO/ Sn-In_2O_3. Further, to enhance the absorptance, we deposited SiO_2 as an anti-reflecting layer and got the optimum absorptance ~ 0.85 and emittance ~ 0.14 for the optimized structures. We also scaled the process to

demonstrate the potential for practical applications and coated one foot long (0.3m) having a one-inch diameter (0.025 m) SS tube. **Figure 7.3(a, b & c)** shows pristine SS tube, optical image taken during dip coating, and coated tubes, respectively. The deposited each layer is dried at 350°C for 5 minutes.

Table 7.1 The estimated absorptance and emittance for the different samples during optimization

Sample	Absorptance	Emittance
ZnO/Sn-In_2O_3)$_{n=2}$/SS	0.76	0.10
ZnO/Sn-In_2O_3)$_{n=4}$/SS	0.80	0.12
ZnO/Sn-In_2O_3)$_{n=6}$/SS	0.82	0.17

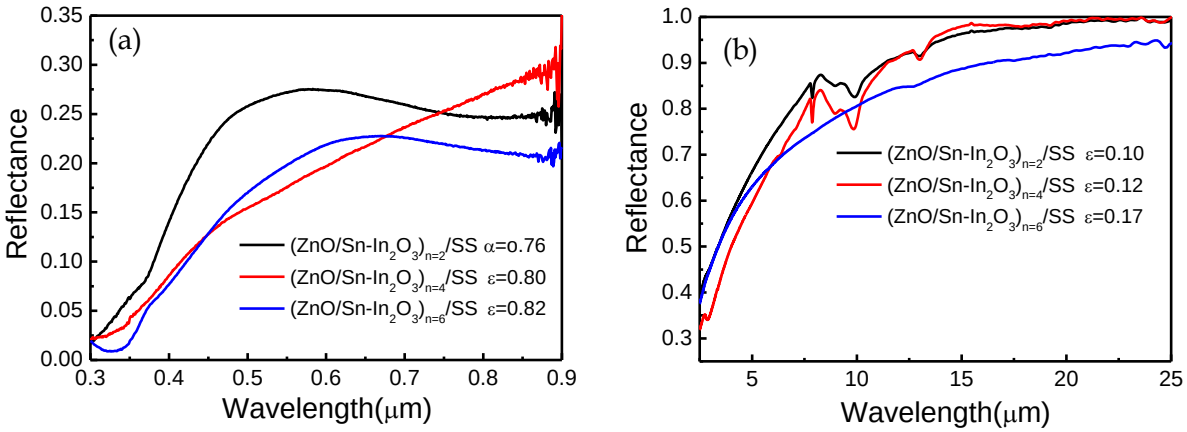

Figure 7.2 Reflectance plot with wavelength for different sample in (a) UV-Vis (0.3-0.9 μm) and (b) IR range (2.5-25 μm)

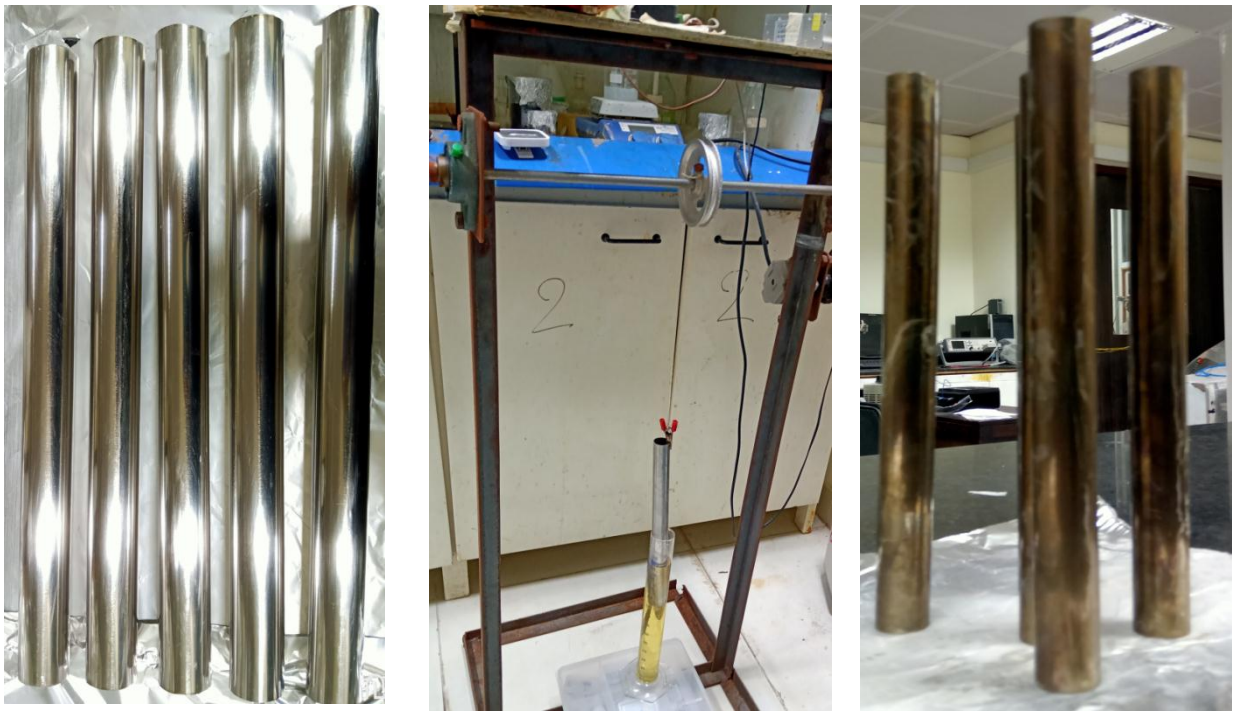

(a) (b) (c)

Figure 7.3 Optical image of SS tube (a) before coating (b) during coating, and (c) after coating

7.4 Result and discussion

The fabricated multilayer structures on SS substrates are investigated using XRD to extract the crystalline information, and the respective XRD plot for optimized coating is shown in **Figure 7.4**. The diffraction peaks at 2θ ~ 30° and 35° correspond to (222) and (400) diffraction planes for Sn-In_2O_3 (consistent with ICDD file No. 06-0416 [Kulkarniet al., 1999, Parsianpour et al., 2017]. The diffraction peaks at 2θ ~ 43, 50, 75 ° correspond to (111), (200), (220) diffractions planes for γ-ferrite (consistent with ICDD file No. 33-0397). The diffraction peaks at 2θ ~ 44, 65° correspond to (110), (200) planes of α-ferrites (ICDD file no 65-4899) [Mathiazhagan et al., 2015, Sha & Lee, 2011]. These ferrite peaks are observed due to the SS substrate. The respective diffraction peaks for the SS substrate and Sn-In_2O_3 are marked for identification in **Figure 7.4**. ZnO and SiO_2 crystalline peaks are not observed in the XRD plot of the fabricated multilayer structure. It might be possible that the ZnO and SiO_2 are present in the amorphous phase.

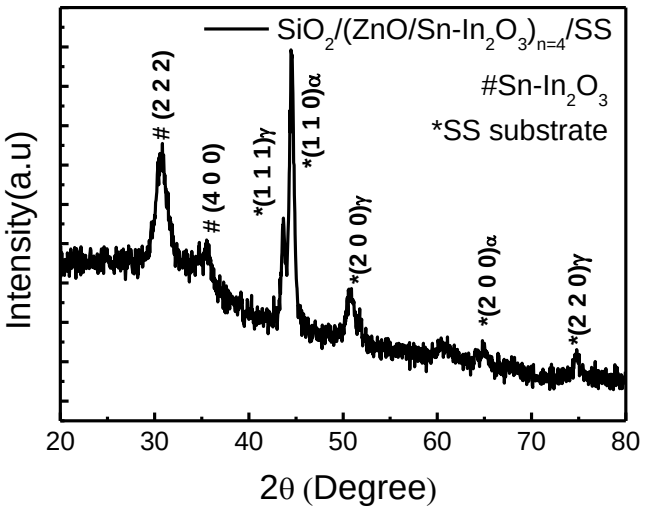

Figure 7.4 XRD plot of fabricated SiO_2/(ZnO/Sn-In_2O_3)$_{n=4}$/SS multilayer structure

Further, the surface morphological properties are investigated using Atomic Force Microscopy (AFM) measurement. **Figures 7.5(a, b, c & d)** show the three-dimensional AFM topographic images for pristine SS substrate, fabricated multilayer sample (optimized one), heat, and corrosion treated samples, respectively. The surface imprints on the pristine SS substrate are visible and attributed to the mechanical polishing of the SS substrate. These surface imprints vanish, and surface seems smooth compared to the pristine SS substrate after depositing multilayer SSACs, Figure **7.5(b)**.. For a heated sample, similar surface micrograph is observed, Figure 7.5(c). However, for the corrosion treed sample, rough terrain was observed, Figure 7.5(d). The surface roughness is also measured and correlated to the optical characteristics of all the four samples. The measured surface roughness (root mean square) for pristine SS was ~ 26.7 nm. The surface roughness was reduced to 7.29 nm for fabricated structure due to the coating of multilayer films. However, for heat and corrosion treated samples, it increases to 16.41 and 33.62 nm, respectively. It is due to the formation of additional surface oxides during thermal and corrosion treatments. The respective roughness of the pristine SS substrate, coated multilayer structure, and thermal as well as corrosion treated samples are mentioned in **Figure 7.5**.

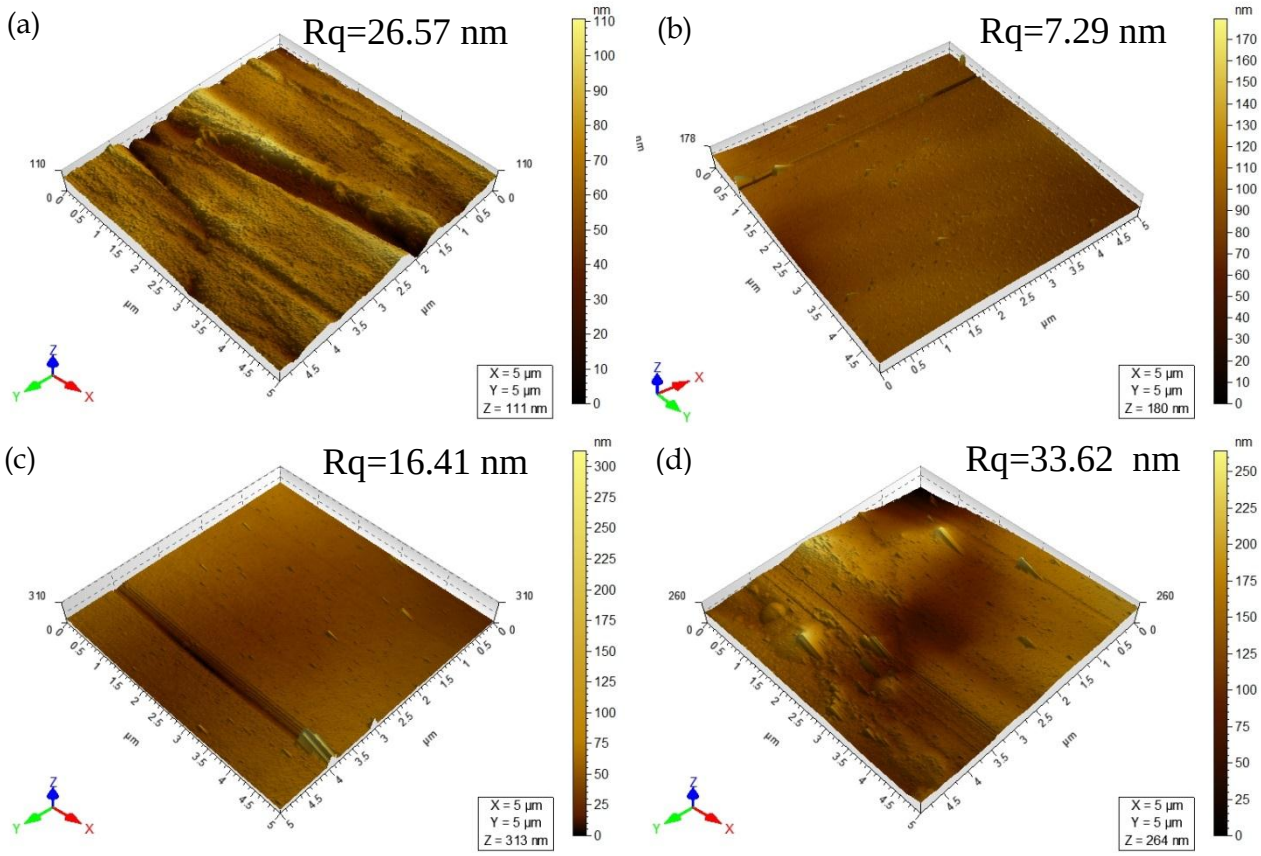

Figure 7.5 3-D AFM image of (a) pristine SS substrate (b) Fabricated SiO2/(ZnO/Sn-In2O3)n=4/SS (c Heat treated and (d) corrosion treated sample

The UV-Vis reflectance measurements are carried out in 0.2 to 0.9 µm ranges and FTIR reflectance in 2.5 to 25 µm to estimate the absorptance and thermal emittance of the fabricated multilayer structure. The representative reflectance plot is shown in **Figure 7.6**. UV-Vis reflectance plot is given in the inset of **Figure 7.6**. The estimated room-temperature emittance is ~ 0.14, whereas the absorptance in UV-Vis range is ~ 0.85 for the optimized sample. The sample is heated in the open air from room temperature to 350°C for 6 hours and then cooled down to room temperature naturally. Fifteen such heating cycles were completed. The schematic of the heat treatment experiment and the heating cycles are shown in **Figures 7.7(a & b)**. After heat treatment, the reflectance in UV-Vis (0.2-0.9 um) and IR range (2.5-25 um) are measured to estimate the absorptance and emittance. The estimated absorptance is nearly identical to the untreated SSAC, whereas the thermal emittance has increased up to ~ 0.18. **Table 7.2** summarizes the optical properties of optimized, heat, and corrosion treated SSAC samples.

Table 7.2 Optical properties of sample A, Sample B and Sample C

Sample	Absorptance	Emittance
Sample A	0.85	0.10
Sample B	0.84	0.14
Sample C	0.83	0.18

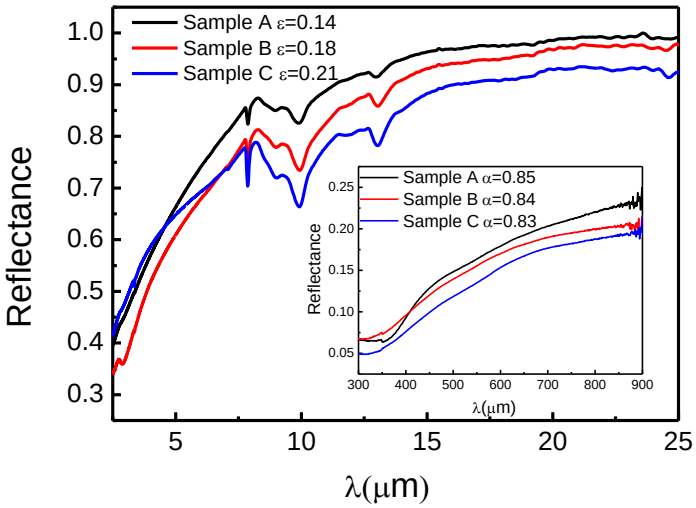

Figure 7.6 Reflectance versus wavelength plot of fabricated SSAC layer (Sample A), heat treated (Sample B) and corrosion treated (Sample C)

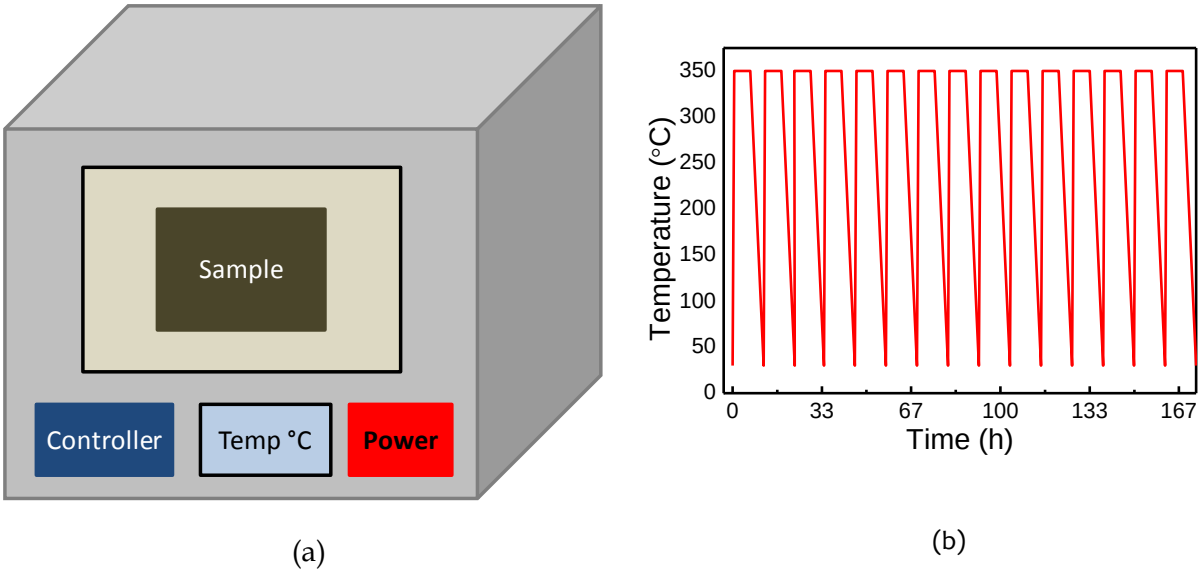

(a) (b)

Figure 7.7 Schematic of (a) Box furnace used for heating (b) Heating cycle of sample

Further, the corrosion measurement was performed for optimized SSAC to study its corrosion-resistant behavior. The electrochemical potentiodynamic measurements were carried out using chemical workstation provide by Autolab (Metrohm) in three-electrode configuration. Ag/AgCl is used as the reference electrode, platinum as the counter electrode, and fabricated layer on SS is used as the working electrode. The 3.5 % NaCl saline solution is used for the corrosion measurements. **Figure 7.8(a & b)** shows the experimental schematic and measured current density versus potential plots. After dipping samples in the saline electrolyte, these were kept in solution for 30 minutes to establish the open-circuit voltage. The observed OCP value for bare SS substrate and SSAC samples are -0.17 and –0.20, respectively. Accordingly, the measurements were performed in -0.5 to 0 V at the scan rate of 10mv/s. NOVA software interfaced with Autolab system is used to estimate the different corrosion parameters. The estimated parameters are summarized in **Table 7.3**. The polarization resistance R_P is measured using Stern-Gray equation in equation (3.1). The breakdown potential for Sample A is more negative as compared to that of SS, and the passive current density is much higher for sample A. The calculated corrosion resistance of sample A is ~ 2.46 kΩ, which is nearly half compared to that of SS ~ 4.28. Also, the corrosion rate for the fabricated sample A is nearly three times higher as compared to pristine SS. These observations suggest that the fabricated structure is less

corrosion resistant in a saline atmosphere with respect to SS. Also the SS itself is a high corrosion resistant alloy. So overall, the fabricated film shows low corrosion resistance compared to SS, but still, the corrosion resistance is quite large. This relatively lower corrosion resistance for SSAC is attributed to the presence of macroscopic cracks on the surface of SSACs. The pre and post heat treatment may cause the evaporation of volatile organic constituents in the film, leading to the macroscopic defects on the surface of SSACs. After the corrosion experiment, the optical properties are estimated using reflectance measurement in UV-Vis and IR range, respectively, as shown in **Figure 7.6.** The observed absorptance for the corrosion treated sample is again not showing any significant changes, but the thermal emittance has increased up to ~0.21. The increase in emittance for corrosion treated sample may be because of enhanced surface roughness and interface mixing/reactions.

Table 7.3 Measured corrosion parameter for pristine SS and Sample A

Sample	E_{corr} (V)	I_{corr} (μA/ cm^{-2})	R_p (kΩ)	C. Rate (mm/y)	b_a (mV/dec)	b_c (mV/dec)
Pristine SS	-207.70	0.383	4.28	0.0043	61.70	75.87
Sample A	-281.28	0.859	2.46	0.015	72.66	111.17

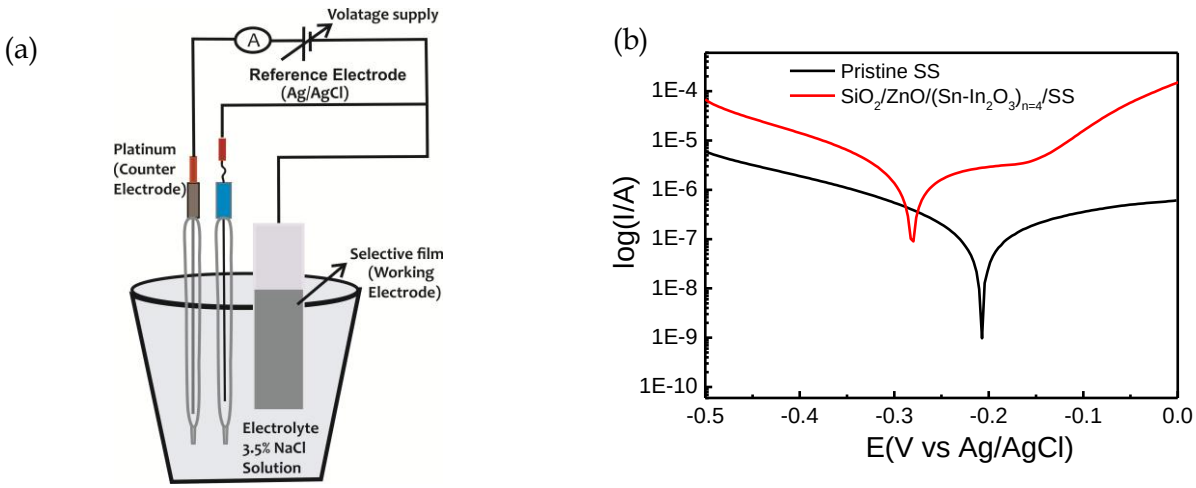

Figure 7.8 (a) Schematic representation of corrosion experiment (b) (a) Potential Vs current density plot for pristine SS and $SiO_2/(ZnO/Sn\text{-}In_2O_3)_{n=4}/SS$

7.5 Conclusion

All oxide-based $SiO_2/(ZnO/Sn\text{-}In_2O_3)_{n=4}/SS$ multilayer structures are developed and optimized for solar thermal performance for the first time using sol-gel dip coating. The structural analysis confirms the presence of $Sn\text{-}In_2O_3$ in the fabricated structure. The process is scaled to demonstrate the coatings on large tubes. The developed film was optically characterized to estimate the absorptance and emittance, and these values for the optimized SSAC structures are ~ 0.85 and 0.14, respectively. The observed absorptance is relatively low (≤ 0.95), and emittance is relatively higher (≥ 0.05) compared to other SSACs for solar thermal applications. It requires further optimization with different low bandgap materials to achieve enhanced solar thermal properties. This study offers a platform to explore all oxide-based coatings for solar thermal applications, which may provide very high thermal and environmental stability. Further, the investigated process is very simple and easily scalable for any surface area and geometry, making it suitable for large scale applications.